



ELSEVIER

Contents lists available at ScienceDirect

## Deep-Sea Research II

journal homepage: [www.elsevier.com/locate/dsr2](http://www.elsevier.com/locate/dsr2)

## Mesoscale features create hotspots of carbon uptake in the Antarctic Circumpolar Current

Elizabeth M. Jones<sup>a,b,\*</sup>, Mario Hoppema<sup>c</sup>, Volker Strass<sup>c</sup>, Judith Hauck<sup>d</sup>, Lesley Salt<sup>e</sup>, Sharyn Ossebaar<sup>b</sup>, Christine Klaas<sup>d</sup>, Steven M.A.C. van Heuven<sup>b</sup>, Dieter Wolf-Gladrow<sup>d</sup>, Tim Stöven<sup>f</sup>, Hein J.W. de Baar<sup>b,g</sup>

<sup>a</sup> Centre for Energy and Environment Sciences, University of Groningen, Nijenborgh 4, 9747 AG Groningen, The Netherlands

<sup>b</sup> Marine Geology and Chemical Oceanography, Royal Netherlands Institute for Sea Research, Landsdiep 4, 1797 SZ Texel, The Netherlands

<sup>c</sup> Alfred-Wegener-Institut Helmholtz-Zentrum für Polar- und Meeresforschung, Climate Sciences Department, Postfach 120161, 27515 Bremerhaven, Germany

<sup>d</sup> Alfred-Wegener-Institut Helmholtz-Zentrum für Polar- und Meeresforschung, Biosciences Department, Postfach 120161, 27515 Bremerhaven, Germany

<sup>e</sup> CNRS, UMR 7144, Equipe Chimie Marine, Station Biologique de Roscoff, Place Georges Teissier, 29680 Roscoff, France

<sup>f</sup> GEOMAR, Helmholtz Centre For Ocean Research, Kiel, Düsternbrooker Weg 20, 24105 Kiel, Germany

<sup>g</sup> Ocean Ecosystems, University of Groningen, Nijenborgh 7, 9747 AG Groningen, The Netherlands

## ARTICLE INFO

## Keywords:

Carbon uptake

Eddies

Polar Front

Antarctic Circumpolar Current

Georgia Basin

## ABSTRACT

The influence of eddy structures on the seasonal depletion of dissolved inorganic carbon (DIC) and carbon dioxide (CO<sub>2</sub>) disequilibrium was investigated during a trans-Atlantic crossing of the Antarctic Circumpolar Current (ACC) in austral summer 2012. The Georgia Basin, downstream of the island of South Georgia (54–55°S, 36–38°W) is a highly dynamic region due to the mesoscale activity associated with the flow of the Subantarctic Front (SAF) and Polar Front (PF). Satellite sea-surface height and chlorophyll-a anomalies revealed a cyclonic cold core that dominated the northern Georgia Basin that was formed from a large meander of the PF. Warmer waters influenced by the SAF formed a smaller anticyclonic structure to the east of the basin. Both the cold core and warm core eddy structures were hotspots of carbon uptake relative to the rest of the ACC section during austral summer. This was most amplified in the cold core where greatest CO<sub>2</sub> undersaturation (−78 μatm) and substantial surface ocean DIC deficit (5.1 mol m<sup>−2</sup>) occurred. In the presence of high wind speeds, the cold core eddy acted as a strong sink for atmospheric CO<sub>2</sub> of 25.5 mmol m<sup>−2</sup> day<sup>−1</sup>. Waters of the warm core displayed characteristics of the Polar Frontal Zone (PFZ), with warmer upper ocean waters and enhanced CO<sub>2</sub> undersaturation (−59 μatm) and depletion of DIC (4.9 mol m<sup>−2</sup>). A proposed mechanism for the enhanced carbon uptake across both eddy structures is based on the Ekman eddy pumping theory: (i) the cold core is seeded with productive (high chlorophyll-a) waters from the Antarctic Zone and sustained biological productivity through upwelled nutrient supply that counteracts DIC inputs from deep waters; (ii) horizontal entrainment of low-DIC surface waters (biological uptake) from the PFZ downwell within the warm core and cause relative DIC-depletion in the upper water column. The observations suggest that the formation and northward propagation of cold core eddies in the region of the PF could project low-DIC waters towards the site of Antarctic Intermediate Water formation and enhance CO<sub>2</sub> drawdown into the deep ocean.

© 2015 Elsevier Ltd. All rights reserved.

## 1. Introduction

The Southern Ocean is a key component in the global meridional overturning circulation through water mass formation, ventilation,

and transport by the Antarctic Circumpolar Current (ACC) between the Atlantic, Pacific and Indian ocean basins (Marshall and Speer, 2012). The ACC is predominantly driven by strong westerly winds where shoaling isopycnal surfaces towards the Antarctic continent enable a direct connection between the surface and the deep ocean and the transfer of carbon dioxide (CO<sub>2</sub>) to the ocean interior (Rintoul et al., 2001; Watson and Orr, 2003; Hauck et al., 2013). The ACC is characterized by a series of circumpolar fronts that are distinguished by strong meridional gradients in hydrographic and biogeochemical parameters (Orsi et al., 1995; Pollard et al., 2002);

\* Corresponding author at: Centre for Energy and Environment Sciences, University of Groningen, Nijenborgh 4, 9747 AG Groningen, The Netherlands; Marine Geology and Chemical Oceanography, Royal Netherlands Institute for Sea Research, Landsdiep 4, 1797 SZ Texel, The Netherlands.

E-mail address: [e.m.jones@rug.nl](mailto:e.m.jones@rug.nl) (E.M. Jones).

<http://dx.doi.org/10.1016/j.dsr2.2015.10.006>

0967-0645/© 2015 Elsevier Ltd. All rights reserved.

the Sub-Tropical Front (STF), the Subantarctic Front (SAF), Polar Front (PF), the Southern ACC Front (SACCF) and the Southern Boundary (SB). Between the STF and SAF are the sub-tropical waters of the Sub-Antarctic Zone (SAZ). The SAF and the PF delimit the sub-Antarctic waters of the Polar Frontal Zone (PFZ). South of the PF is the Antarctic Zone (AAZ). Inverse modelling suggests that the CO<sub>2</sub> sink of the Southern Ocean is sensitive to climate change as wind intensification can lead to increased upwelling of deep waters rich in natural CO<sub>2</sub> (Le Quéré et al., 2007; Law et al., 2008; Lovenduski et al. (2008); Zickfeld et al., 2008). In contrast, hydrographic data indicates that transport and meridional overturning circulation in the ACC is not very sensitive to increasing winds (Böning et al., 2008) due to mesoscale (principally eddy) activity in the ACC being inadequately resolved by numerical simulations. Hence gaps persist in the understanding of the role of eddies on CO<sub>2</sub> uptake in the ACC.

Mesoscale structures, such as meandering hydrographic fronts, currents, eddies and topographically induced turbulence, are ubiquitous in the ACC. Such structures are linked to enhanced entrainment, retention, mixing, biological production and transport of heat, salt, carbon and nutrients within the ACC (McGillicuddy and Robinson, 1997; Siegel et al., 1999). Mesoscale eddies are conspicuous structures, typically up to 50 km in radius (of the order of the first baroclinic Rossby radius), and can be detected by anomalies in sea surface height and temperature. Eddies contribute to distinct patchiness in the upper ocean by affecting the spatio-temporal distribution of sea surface chlorophyll-a and productivity of phytoplankton through the uplift or subduction of isopycnals and nutriclines (Strass, 1992; Kimura et al., 1997; McGillicuddy et al., 1998; Lee and Williams, 2000; Lévy, 2003; Klein and Lapeyre, 2009; Saraceno and Provost, 2012) and they play an important role in the ACC component of the global overturning circulation (Thompson et al., 2014). The concept of 'eddy pumping' states that vertical motions within the eddy cores produces anomalies in sea surface height and temperature (McGillicuddy et al., 1998; Klein and Lapeyre, 2009). Cold core (cyclonic) eddies lead to a doming of isopycnals and upwell cold, nutrient-rich deep water into the euphotic zone (McGillicuddy and Robinson, 1997). Cold core eddies can be detected by satellite as negative sea surface height and are often associated with increased biological productivity (Falkowski et al., 1991; Robinson et al., 1993; Allen et al., 1996; McGillicuddy et al., 1998). Warm core (anticyclonic) eddies can be detected by an elevated sea surface height (positive sea level anomaly) and are vortices of anticlockwise rotating water leading to a deepening of isopycnals and downwelling of surface waters, which are relatively unproductive (McGillicuddy and Robinson, 1997; McGillicuddy et al., 1998).

However, other mechanisms such as deepening mixed layers and horizontal advection can result in productive anticyclonic eddies (Dufois et al., 2014). The objective of this study is to understand the role of eddies on the biological carbon uptake in the ACC (e.g., Moore and Abbott, 2000; Strass et al., 2002; Sokolov and Rintoul, 2007; Le Quéré et al., 2007; Böning et al., 2008) and the wider impact of eddies on the sensitivity of the carbon cycle to climate change in the Southern Ocean.

Remotely sensed chlorophyll-a and sea surface height showed high levels of mesoscale activity downstream (to the north) of the island of South Georgia (54–55°S, 36–38°W) in the Atlantic sector of the Southern Ocean (Korb et al., 2004; Borriane and Schlitzer, 2013). Shipboard surveys have revealed finer scale topographic interactions of the SAF, PF and SACCF with the Scotia Ridge that leads to meandering and the formation of eddy structures in the Georgia Basin (Trathan et al., 1997; Meredith et al., 2003; Korb and Whitehouse, 2004; Smith et al., 2010). The waters in the Georgia Basin support vast phytoplankton blooms that develop each year and often persist for 04 months or more, characterising the region as one of the most biologically productive areas in the Southern Ocean (Atkinson et al., 2000; Korb and Whitehouse, 2004; Korb et al., 2004; Borriane and Schlitzer, 2013). Enhanced biological uptake of CO<sub>2</sub> occurs from spring to summer to autumn in the large South Georgia blooms (Jones et al., 2012, 2015; Jones et al., in press).

Persisting mesoscale activity and eddy formation mechanisms associated with the meandering of the PF and SAF make the Georgia Basin an ideal location to explore the effects of eddy dynamics on the uptake and cycling of CO<sub>2</sub> in the ACC. Anomalies in remotely sensed sea surface topography and chlorophyll-a in austral summer 2012 revealed the presence of an eddy dipole structure downstream of South Georgia. Shipboard hydrographic measurements confirmed the existence of a large (~400 km diameter) cyclonic cold core in the northern Georgia Basin with warmer waters to the east forming a smaller anticyclonic core (Strass et al., in this issue). Effects of the mesoscale eddy structures on the seasonal depletion of inorganic carbon and the summertime CO<sub>2</sub> disequilibrium are investigated. The data comprise shipboard continuous and discrete measurements of the CO<sub>2</sub> system and MODIS-Aqua ocean colour and altimetry data. Results from these measurements are put into context by reference to the whole trans-Atlantic passage and the potential of eddies to create 'hotspots' of carbon uptake in the ACC is inferred.

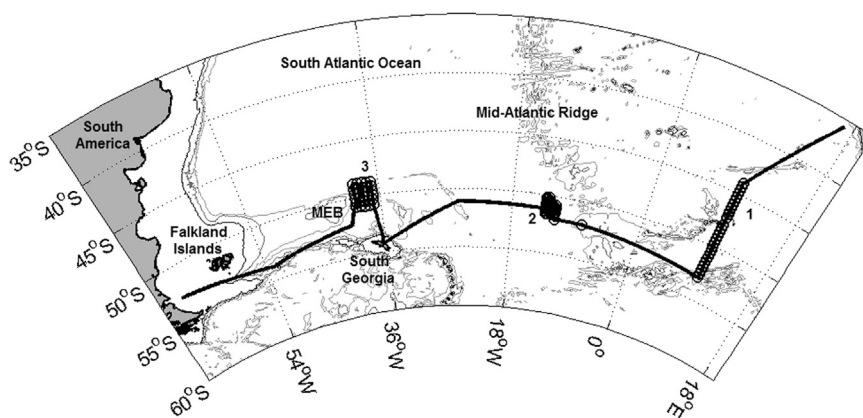


**Fig. 1.** Map of the ANT-XXVIII/3 cruise track in the South Atlantic and Southern Ocean. The surveyed regions are depicted by clusters of hydrographic stations (black open circles) and labelled numerically as: (1) a section along 44–53°S, 10°E (stations 57–84); (2) mesoscale survey at 50–52°S, 12–13.5°W west of the Mid-Atlantic Ridge (stations 87–142); (3) mesoscale survey at 48.5–51.5°S, 37–39.5°W in the Georgia Basin (stations 144–173). South Georgia island, Mid-Atlantic Ridge, Maurice-Ewing Bank (MEB) and the Falkland Islands are marked on the map.

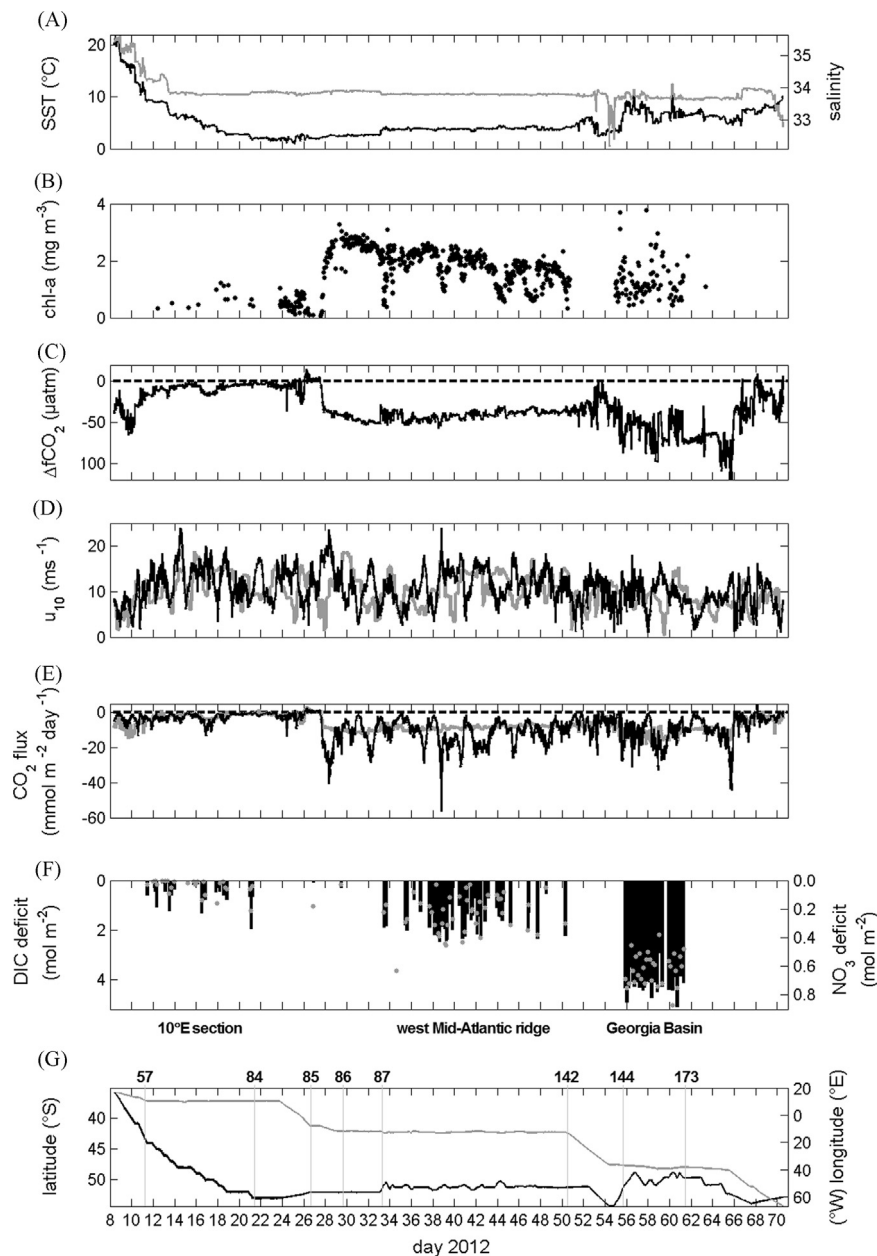


**Fig. 2.** ANT-XXVIII/3 underway hydrological and meteorological parameters with respect to day (2012): (a) sea surface temperature (SST, °C; black), sea surface salinity (grey); (b) chlorophyll-a ( $\text{mg m}^{-3}$ ); (c)  $\Delta\text{fCO}_2$  ( $\mu\text{atm}$ ); (d) ship (black) and NCEP re-analysis data (grey) of wind speed ( $u_{10}$ ,  $\text{m s}^{-1}$ ); (e) air-sea  $\text{CO}_2$  flux using ship (black) and monthly means of NCEP re-analysis data (grey) wind speed ( $\text{mmol m}^{-2} \text{ day}^{-1}$ ); (f) DIC deficit ( $\text{mol m}^{-3}$ ; black bars),  $\text{NO}_3$  deficit ( $\text{mol m}^{-3}$ ; grey dots); (g) latitude ( $^{\circ}\text{S}$ ; black), longitude ( $^{\circ}\text{W}$ ; grey). Horizontal dashed lines mark 0  $\Delta\text{fCO}_2$  and 0  $\text{CO}_2$  flux where data below represent  $\text{CO}_2$  undersaturation and a  $\text{CO}_2$  sink, respectively. The vertical grey lines de-limit the main surveyed regions with key stations labelled: (1) 10°E section (stations 57–84); (2) mesoscale survey west of the Mid-Atlantic Ridge (stations 87–142); (3) mesoscale survey in the Georgia Basin (stations 144–173).

## 2. Methods

### 2.1. Oceanographic setting and station sampling

A biogeochemical survey of the Atlantic sector of the Southern Ocean was conducted from 07 January to 11 March 2012 during expedition ANT-XXVIII/03 on FS *Polarstern* (Wolf-Gladrow, 2013). Satellite altimetry and ocean colour data were used onboard to identify mesoscale features along the ships track from Cape Town, South Africa, to Punta Arenas, Chile. Three sub-regions were studied in detail: (1) a section along 44–53°S, 10°E; (2) a mesoscale survey at 50–52°S, 12–13.5°W west of the Mid-Atlantic Ridge; (3) a mesoscale survey at 48.05–51.5°S, 37–39.5°W in the Georgia Basin (Fig. 1). Numerous measurements were made alongside the

conductivity, temperature, depth (CTD, SeaBird SBE 911plus) surveys in each of the sub-regions (Fig. 2). Vertical profiles of potential temperature ( $\theta$ ) and salinity were obtained from the CTD downcast at each station and were used to determine the summer mixed layer depth (mld) at each station (Strass et al., in this issue). Shipboard meteorological parameters were continually recorded from sensors located at 39 m above sea level and hydrographic parameters were frequently measured from the underway seawater supply, with an intake located at 8 m depth. All salinity values are reported on the practical salinity scale. Satellite altimetry data is presented as merged absolute dynamic topography (Fig. 3) where the main hydrographic fronts (SAF, PF, SACCF) of the region were identified based on the definitions by Venables et al. (2012). The altimeter products were produced by Ssalto (Segment

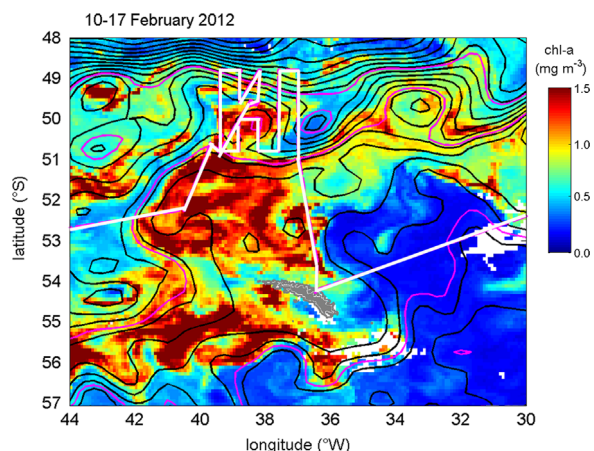


**Fig. 3.** MODIS-Aqua chlorophyll-a ( $\text{mg m}^{-3}$ ) composite image from 10–17 February 2012 with merged absolute dynamic topography contours (dyn cm, black) and the cruise track (white) overlain. Pink lines denote locations of (from north to south) the main path of the SAF, PF and SACCF, as defined by Venables et al. (2012). The island appearing in the image is South Georgia. (For interpretation of the references to colour in this figure legend, the reader is referred to the web version of this article.)

Sol multi-missions d'Altimétrie, d'orbitographie et de localisation précise)/Duacs (Data unification and Altimeter combination system) and distributed by Aviso (Archiving, Validation and Interpretation of Satellite Oceanographic data), with support from Cnes (Centre National d'Etudes Spatiales); <http://www.aviso.altimetry.fr/duacs/>. Hydrographic stations are classified based on physical characteristics of the Sub-Antarctic Zone (SAZ), the Polar Frontal Zone (PFZ) and Antarctic Zone (AAZ) including warm core (w/core) and cold core (c/core) eddy structures (Table 1; Fig. 4).

## 2.2. Marine chemical parameters

Samples for dissolved inorganic carbon (DIC) and macronutrients (silicate, phosphate, nitrite and nitrate) were collected from  $24 \times 12$  L Niskin bottles mounted on the CTD rosette. Seawater (500 mL) for DIC analysis was collected in borosilicate glass bottles and analysed within 20 hours using a VINDTA 3 C (Versatile Instrument for the Determination of Total Alkalinity, Marianda, Kiel) instrument. The DIC concentration was determined by coulometric analysis (Johnson et al., 1987) with calibration performed at the start and end of each measurement cycle (typically one cycle refers to one full depth hydrographic station) with certified reference materials (CRM, batch 113) (Dickson et al., 2007, 1981). The precision of the DIC measurements is  $1.04 \mu\text{mol kg}^{-1}$ , based on the average difference between all CRM in-bottle duplicate analyses. The accuracy is estimated as  $2.00 \mu\text{mol kg}^{-1}$ , based on the average difference between measured CRM raw and corrected DIC values. For macronutrient assays, seawater (125 mL) was collected in polypropylene bottles and transferred into 05 mL polyethylene vials and analysed within 15 h of sampling using a Technicon TRAACS 800 Auto-analyzer. All samples and standards were brought to laboratory temperature of  $22^\circ\text{C}$  in approximately two hours prior to analysis. During each run a daily freshly diluted nutrient standard containing silicate, phosphate and nitrate was measured in triplicate. Additionally, a natural sterilised Reference Material Nutrient Sample (JRM Kanso, Japan) containing known concentrations of silicate, phosphate and nitrate was analysed in triplicate every 02 weeks. The house standard and the JRM were both used to monitor the performance of the analyzer, where the precision for silicate, phosphate and nitrate is determined as  $0.06 \mu\text{mol L}^{-1}$ ,  $0.016 \mu\text{mol L}^{-1}$ ,  $0.13 \mu\text{mol L}^{-1}$ , respectively.

Depth-integrated nitrate and DIC deficits were calculated from vertical profiles relative to the concentration at 100 m depth (Table 1); nutrient deficits for this cruise are also presented in Hoppe et al. (this issue). Vertical integration to 100 m depth was selected from the average depth of the Winter Water potential temperature minimum ( $\theta_{\text{min}}$ ), which was clearly visible in the depth range 100–150 m for stations south of the Polar Front (Fig. 5a). Depth-integrated DIC deficits relative to the concentration at 150 m depth reveal similar trends; high DIC deficits generally occurred within both the cold and warm cores with a maximum DIC deficit in the cold core. However, there was a large disparity in the absolute values of some of the deficits for those two reference depths. For example, all cold core stations showed DIC deficits enhanced by 13–47% when 150 m was used as the reference depth instead of 100 m and for warm core stations the equivalent difference was 01–8%. This largely reflects the influence of the cyclonic uplift of DIC-rich waters in the cold core in the upper 250 m. In contrast, the choice of reference depth for the value of DIC deficits in the warm core is less critical. Therefore, 100 m is a more conservative choice as the reference depth to determine DIC-deficits as the seasonal depletion in inorganic carbon. This depth was also used for stations north of the PF, with no visible potential temperature minimum, in order to be consistent within this study and comparable to other studies in the Southern Ocean and ACC region (e.g., Bates et al., 1998; Sweeney et al., 2000; Bakker et al., 2007; Jones et al., 2012). It is assumed that the 100 m DIC concentration represents the Winter Water reference and no significant lateral or vertical exchanges of DIC have taken place at this depth. It is recognised that this is not totally valid in the turbulent ACC, hence the resultant deficit values are compared more on a regional basis and not station by station.

## 2.3. Air–sea $\text{CO}_2$ fluxes

Quasi-continuous determinations of the fugacity of  $\text{CO}_2$  ( $f\text{CO}_2$ ) in surface water from the ships underway seawater supply and in marine air were made using a General Oceanics system (GO 8050). Marine air samples were taken from an air inlet located forward on FS *Polarstern* at 39 m height. Mixing ratios of  $\text{CO}_2$  and moisture in the marine air and equilibrator headspace were determined by infrared detection with a LI-COR 7000 as part of the GO 8050 system. The LI-COR was calibrated using secondary gas standards with nominal  $\text{CO}_2$  concentrations of 200, 400 and 750 ppm and nitrogen was used as the zero reference gas. The  $f\text{CO}_2$  was computed from the dried mixing ratios and the ship's barometric pressure and then corrected for seawater vapour pressure (Weiss and Price, 1980). Sea surface  $f\text{CO}_2$  data were corrected to sea surface temperature to account for warming upon passage through the ship (Takahashi et al., 1993, 2009). The precision of the  $f\text{CO}_2$  data is estimated at better than  $02 \mu\text{atm}$ . Sea surface  $\text{CO}_2$  disequilibrium ( $\Delta f\text{CO}_2$ ) is determined from the gradient of  $f\text{CO}_2$  across the air–sea interface ( $f\text{CO}_{2\text{sea}} - f\text{CO}_{2\text{air}}$ ). Air–sea fluxes of  $\text{CO}_2$  were calculated along the ships track from  $\Delta f\text{CO}_2$  and the gas transfer relationship of Nightingale et al., 2000 using (i) shipboard wind speeds corrected to 10 m altitude ( $u_{10}$ ; Hartman and Hammond, 1985) and (ii) monthly means of the NCEP 06-hourly, 10 m wind speed product (Kalnay et al., 1996) during the study period. The two calculated flux values thus allow a comparison of instantaneous  $\text{CO}_2$  fluxes from shipboard winds and  $\text{CO}_2$  fluxes representative of monthly mean wind speeds from re-analysis data (Table 1). Negative values of  $\Delta f\text{CO}_2$  and  $\text{CO}_2$  flux indicate  $\text{CO}_2$  undersaturation with respect to the atmosphere and therefore net uptake of atmospheric  $\text{CO}_2$ .

**Table 1**

ANT-XXVIII/3 station information and selected biogeochemical data: station number; latitude (°S); longitude (°W); sampling day in 2012; time (*t*) since start of growing season; average mixed layer chlorophyll-*a* (chl-*a*, mg m<sup>-3</sup>); CO<sub>2</sub> disequilibrium ( $\Delta f\text{CO}_2$ ,  $\mu\text{atm}$ ); DIC deficit (mol m<sup>-2</sup>);  $\delta\text{DIC}/\delta t$  (mol m<sup>-2</sup> day<sup>-1</sup>); air-sea CO<sub>2</sub> flux (mmol m<sup>-2</sup> d<sup>-1</sup>) from shipboard wind speeds and, in parentheses, fluxes from NCEP re-analysis wind speeds. No data marked by -. Data highlighted with \* indicate a 'hotspot' as defined as a magnitude equal to or exceeding the average + one standard deviation.

Station	Latitude °S	Longitude °W	Day	<i>t</i> days	chl- <i>a</i> mg m <sup>-3</sup>	$\Delta f\text{CO}_2$ $\mu\text{atm}$	DIC deficit mol m <sup>-2</sup>	$\delta\text{DIC}/\delta t$ mmol m <sup>-2</sup> day <sup>-1</sup>	CO <sub>2</sub> flux mmol m <sup>-2</sup> d <sup>-1</sup>
57	-44.0012	10.0040	11	103	-	-15	0.6	5.7	-3.5 (-3.4)
58	-44.3367	10.0015	12	104	-	-7	-	-	-3.6 (-1.7)
59	-44.6685	10.0018	12	104	-	-8	0.4	4.2	-1.5 (-2.0)
60	-44.9987	9.9985	12	104	0.3	-11	1.1	10.3	-3.8 (-2.5)
62	-45.6755	10.0077	12	104	-	-8	0.1	1.0	-2.5 (-1.8)
63	-46.0087	10.0013	13	105	0.3	-11	0.4	4.3	-3.6 (-2.5)
64	-46.3378	10.0007	13	105	-	-18	-	-	-3.3 (-4.3)
65	-46.6668	10.0015	13	105	-	-12	1.2	11.7	-1.3 (-2.9)
66	-46.9993	10.0082	13	105	0.6	-7	0.6	5.6	-1.2 (-1.6)
67	-47.3332	9.9985	14	105	-	-9	0.3	3.2	-3.6 (-2.2)
69	-47.9963	10.0065	15	107	0.4	-3	0.1	1.0	-0.6 (-0.8)
70	-48.3343	10.0002	15	107	-	-3	0.2	1.7	-1.6 (-0.8)
71	-48.6672	10.0055	15	107	-	-2	0.0	0.1	-0.9 (-0.5)
72	-49.0000	10.0040	16	108	0.4	-5	0.1	1.2	-2.0 (-1.3)
73	-49.3428	10.0072	16	108	-	-13	1.3	12.2	-5.2 (-3.5)
74	-49.6667	10.0023	16	108	-	-15	0.4	3.6	-5.7 (-3.8)
75	-50.0005	9.9993	16	108	0.9	-16	0.8	7.0	-8.3 (-2.8)
76	-50.3298	10.0232	17	109	1.0	-12	0.5	4.4	-1.6 (-1.7)
77	-50.6647	10.0000	17	109	1.1	-7	0.2	2.3	-0.3 (-1.6)
78	-51.0017	9.9992	18	110	1.2	-7	0.4	4.1	-2.0 (-1.6)
79	-51.3360	9.9998	18	110	1.1	-7	0.6	5.3	-3.6 (-1.1)
80	-51.6687	10.0037	18	110	0.6	-6	0.4	4.1	-4.1 (-1.5)
81	-51.9990	10.0048	18	110	0.6	-5	0.8	7.0	-2.4 (-1.2)
82	-52.3448	10.0005	20	112	0.5	-2	0.7	5.8	-0.3 (-0.6)
83	-52.6665	10.0027	21	113	0.6	-4	2.0	17.3	-0.6 (-0.8)
84	-52.9977	10.0013	21	113	0.4	-4	0.7	5.8	-0.8 (-1.0)
85	-51.9983	-8.0042	26	118	0.1	3	0.0	0.0	1.2 (0.8)
86	-51.9970	-11.9762	29	121	2.6	-41	0.3	2.3	-13.3 (-10.0)
87	-50.8365	-13.1553	33	125	0.6	-36	1.9	15.1	-8.5 (-7.4)
88	-50.3333	-13.1662	33	125	1.5	-42	1.8	14.6	-10.2 (-8.7)
91	-51.2127	-12.6733	34	126	2.0	-36	-	-	-4.8 (-7.5)
92	-50.7988	-12.6647	35	127	2.2	-49	1.8	14.3	-4.3 (-10.1)
93	-50.8085	-12.6693	35	127	-	-51	2.0	15.9	-3.6 (-10.5)
95	-51.1980	-12.0015	36	128	2.3	-44	0.8	6.1	-12.8 (-9.0)
96	-51.1998	-12.3307	36	128	2.3	-47	-	-	-8.6 (-9.7)
98	-51.2058	-12.6637	36	128	2.2	-48	1.3	9.9	-11.4 (-9.9)
101	-51.3997	-12.6660	37	129	2.4	-47	1.9	14.6	-7.2 (-9.7)
102	-51.5967	-12.6665	37	129	2.3	-44	1.3	9.8	-3.9 (-9.2)
103	-51.6017	-12.9975	38	130	-	-46	2.2	16.8	-2.8 (-9.5)
104	-51.6005	-13.3317	38	130	2.4	-45	0.7	5.2	-5.0 (-9.3)
105	-51.3998	-13.3317	38	130	-	-57*	2.2	17.2	-16.7 (-11.8)
106	-51.2007	-13.3315	38	130	1.7	-52	2.5	18.9	-16.5 (-10.9)
107	-51.0018	-13.3292	38	130	-	-43	1.9	14.3	-25.0 (-8.9)
108	-50.7985	-13.3308	38	130	1.1	-42	1.8	13.8	-16.7 (-8.8)
109	-50.7997	-12.9987	39	131	-	-42	2.0	14.9	-14.6 (-8.7)
110	-50.9995	-12.9973	39	131	-	-46	2.4	18.5	-16.8 (-9.6)
111	-51.1970	-12.9985	39	131	1.6	-48	2.4	18.1	-26.5 (-9.9)
112	-51.4003	-12.9952	39	131	-	-42	0.9	7.2	-14.8 (-8.8)
114	-51.1993	-12.6690	39	131	2.2	-41	2.0	15.1	-16.1 (-8.6)
115	-50.9985	-12.6645	40	132	1.8	-45	1.0	7.7	-20.3 (-9.4)
116	-50.7985	-12.6603	40	132	1.3	-45	2.3	17.8	-23.4 (-9.4)
117	-50.8000	-12.3330	40	132	-	-47	2.3	17.0	-2.5 (-9.8)
118	-51.0007	-12.3322	41	133	-	-39	0.7	5.4	-3.8 (-8.0)
119	-51.2022	-12.3342	41	133	2.1	-39	1.4	10.2	-5.6 (-8.0)
120	-51.4015	-12.3328	41	133	-	-39	0.2	1.6	-9.2 (-8.0)
121	-51.5992	-12.3303	41	133	-	-40	1.6	12.0	-8.9 (-8.3)
122	-51.5978	-11.9965	41	133	1.8	-39	1.4	10.6	-12.8 (-8.0)
123	-51.4010	-11.9993	41	133	-	-42	0.7	5.3	-24.5 (-8.7)
124	-51.2000	-11.9970	42	134	2.1	-42	2.2	16.1	-21.6 (-8.7)
125	-51.0000	-11.9992	42	134	-	-41	1.5	10.8	-20.4 (-8.5)
126	-50.7998	-11.9990	42	134	1.7	-44	2.3	17.3	-17.9 (-9.2)
127	-51.2302	-12.4127	42	134	2.0	-42	1.7	12.4	-20.6 (-8.7)
128	-51.2005	-12.6623	43	135	1.6	-41	0.7	5.3	-18.9 (-8.4)
129	-50.5990	-13.0010	43	135	-	-40	1.1	8.1	-4.4 (-8.2)
130	-50.4002	-12.9993	44	136	0.9	-33	-	-	-3.8 (-6.9)
131	-50.2013	-13.0065	44	136	0.8	-38	1.4	10.6	-5.5 (-7.9)
132	-50.2000	-13.3343	44	136	-	-36	1.5	10.9	-5.6 (-7.5)
133	-50.4003	-13.3335	44	136	0.7	-34	1.6	11.9	-6.5 (-7.0)
134	-50.5985	-13.3335	44	136	0.7	-33	0.9	6.3	-6.2 (-6.8)
136	-51.2003	-12.6655	45	137	1.4	-37	1.8	13.4	-9.3 (-7.6)
137	-51.0362	-12.1722	46	138	1.7	-37	1.3	9.2	-7.1 (-7.7)

Table 1 (continued)

Station	Latitude °S	Longitude °W	Day	t days	chl-a mg m <sup>-3</sup>	ΔfCO <sub>2</sub> μatm	DIC deficit mol m <sup>-2</sup>	δDIC/δt mmol m <sup>-2</sup> day <sup>-1</sup>	CO <sub>2</sub> flux mmol m <sup>-2</sup> d <sup>-1</sup>
139	-50.9932	-12.9892	46	138	0.8	-35	2.0	14.4	-5.0 (-7.3)
140	-51.2003	-12.6645	47	139	1.7	-40	2.3	16.8	-8.0 (-8.3)
141	-51.1995	-12.6120	48	140	1.4	-39	0.5	3.8	-18.7 (-8.1)
142	-51.1988	-12.6683	50	142	1.0	-35	2.2	15.7	-8.8 (-7.3)
144	-50.7942	-36.9777	55	147	1.8	-79*	4.3*	29.5	-9.5 (-16.1)
145	-50.3935	-36.9973	56	148	-	-59*	4.9*	33.1	-12.1 (-11.9)
146	-50.0018	-37.0010	56	148	-	-49	4.3*	29.3	-12.8 (-10.0)
147	-49.6058	-37.0140	56	148	-	-52	3.5	23.5	-12.0 (-10.5)
148	-49.1965	-36.9668	56	148	-	-50	4.1*	27.4	-13.8 (-10.1)
149	-48.8022	-36.9830	56	148	-	-41	4.3*	29.0	-7.5 (-8.3)
150	-48.8050	-37.5858	56	148	-	-45	3.4	22.8	-10.6 (-9.2)
151	-49.1990	-37.5940	57	149	-	-49	4.1*	27.6	-10.1 (-9.9)
152	-49.6063	-37.5953	57	149	1.8	-70*	4.3*	28.9	-16.7 (-14.3)
153	-50.0025	-37.6092	57	149	1.0	-55	4.2*	28.5	-17.9 (-11.2)
154	-50.4042	-37.6045	57	149	0.8	-53	4.4*	29.7	-8.4 (-10.7)
155	-50.8100	-37.5773	57	149	0.9	-53	4.3*	28.9	-5.3 (-10.8)
156	-50.8142	-38.1948	57	149	3.8	-86*	3.8*	25.4	-4.6 (-17.6)
157	-50.4068	-38.1892	58	150	1.0	-55	4.1*	27.1	-0.4 (-11.2)
158	-50.0000	-38.2182	58	150	1.0	-51	4.1*	27.3	-2.9 (-10.4)
159	-49.9958	-38.8110	58	150	2.0	-73*	4.7*	31.6	-16.7 (-14.9)
160	-50.3970	-38.8008	58	150	1.2	-56	3.4	23.0	-17.8 (-11.6)
161	-50.8010	-38.7952	58	150	1.2	-61*	4.1*	27.3	-14.2 (-12.6)
162	-50.7967	-39.4158	58	150	1.6	-75*	4.5*	29.9	-22.5 (-15.5)
163	-50.4013	-39.3993	59	151	0.6	-38	2.9	19.3	-17.7 (-7.9)
164	-49.9985	-39.4027	59	151	1.9	-66*	4.3*	28.4	-25.5 (-13.6)
165	-49.6010	-39.4013	59	151	1.7	-72*	4.4*	29.1	-9.1 (-14.8)
166	-49.2000	-39.3982	60	152	1.2	-51	3.5	23.1	-8.3 (-10.6)
167	-48.7895	-39.3222	60	152	-	-46	4.4*	29.1	-14.4 (-9.2)
168	-48.7960	-38.7347	60	152	-	-48	3.9*	25.6	-9.6 (-9.6)
169	-49.1998	-38.8005	60	152	0.7	-42	3.5	23.0	-7.3 (-8.5)
170	-49.6025	-38.7978	60	152	1.9	-78*	5.1*	33.5	-15.6 (-15.8)
171	-48.7962	-38.1482	60	152	-	-54	3.8*	25.3	-7.8 (-11.0)
172	-49.2048	-38.2032	61	153	0.7	-41	3.7*	24.3	-2.6 (-5.4)
173	-49.5978	-38.2060	61	153	1.5	-72*	4.1*	26.9	-9.0 (-9.4)
						-38	2.1	<b>Average</b>	
						20	1.5	<b>Std dev</b>	
						-58	3.6	<b>'Hotspot'</b>	

#### 2.4. Satellite and shipboard chlorophyll-a

MODIS-Aqua ocean colour data were obtained from NASA (<http://oceancolor.gsfc.nasa.gov>) as 08 day, 09 km, level 03 mapped data with contours of merged absolute dynamic topography overlain (Fig. 3). Water samples for chlorophyll-a determination were obtained from the CTD Niskin bottles at 08 to 10 depths from the surface down to 200 m depth. In addition, sea surface samples for chlorophyll-a analysis were collected at 30–60 min intervals from the ship's underway seawater supply. All samples were filtered onto 25 mm diameter GF/F filters at pressures not exceeding 200 mbar. Filters were immediately transferred to centrifuge tubes with 10 mL 90% acetone and 01 cm<sup>3</sup> of glass beads. The tubes were sealed and stored (cooled) at -20 °C for at least 30 min and up to 24 h. Chlorophyll-a was extracted by placing the centrifuge tubes in a grinder for 3 min followed by centrifugation at 0 °C. The supernatant was poured in quartz tubes and measured for chlorophyll-a content in a Turner 10-AU fluorometer. Calibration of the fluorometer was carried out at the beginning and at the end of the cruise. Results of the fluorometer calibration diverged by 2% between beginning and end of the cruise. Chlorophyll-a content was calculated using the equation given in Knap et al. (1996) using average parameter values from the two calibrations. Chlorophyll data are also presented in Hoppe et al., in this issue.

### 3. Results

#### 3.1. The Atlantic ACC during summer: a physical and biological perspective

Surface physical and biological data are first presented from the whole Atlantic crossing from Cape Town on 7 January to Punta Arenas on 11 March 2012 (Fig. 2) in chronological order to provide a basin-wide perspective of summertime patterns and processes in the ACC, from which effects on oceanic CO<sub>2</sub> uptake are determined. Maximum sea surface temperature and salinity occurred north of 45°S (day 8–10) on the south-westerly passage from Cape Town to the start of the 10°E section (Fig. 2a). Between 45.7–47.0°S (stations 62–66) sharp decreasing sea surface temperature is evident, identifying the SAF at 46.5 °S. The poleward decrease in sea surface temperature along the 10°E section appeared to culminate with surface gradients of decreasing temperature and a slight increase in salinity at about 50.5°S. The transition to saltier, ~2 °C surface waters represents the surface expression of the PF (stations 82–83). A slight increase in surface salinity at about 52.5°S marks the SACCF, accompanied by colder Winter Water temperatures (Strass et al., in this issue). Along the 10°E section, sea surface chlorophyll-a was consistently higher than 0.3 mg m<sup>-3</sup>, peaking at 1.2 mg m<sup>-3</sup> at station 78 (day 18).

After the North-South transect at 10°E the ship headed westward for a mesoscale survey at 12–13.5°W 50–52°S west of the Mid-Atlantic Ridge (Fig. 1). Sea surface chlorophyll-a concentrations steadily decreased on the westward passage, with the

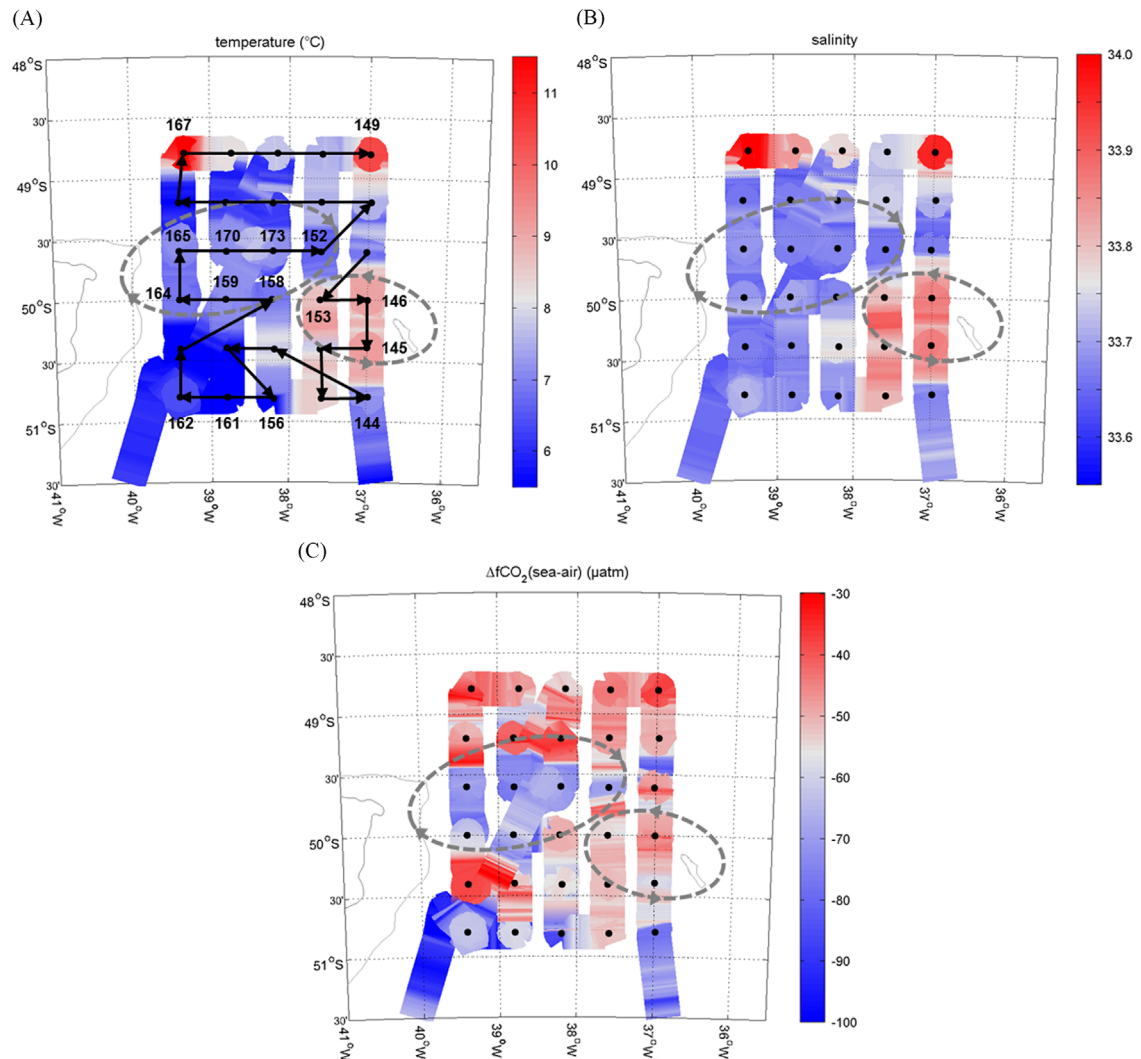


**Fig. 4.** Sea surface plots of (a) temperature (SST, °C), (b) salinity, and (c)  $\Delta f\text{CO}_2$  ( $\mu\text{atm}$ ) during the mesoscale survey in the Georgia Basin. General flow vectors marking areas of clockwise cyclonic (cold core) and anti-clockwise anti-cyclonic (warm core) motions are indicated (Strass et al., in this issue) with relevant stations labelled. For upper ocean sections in Fig. 5 the order of station data displayed is indicated by the solid black arrows.

exception of two blooms at 1.4–0.6°E (day 25) and 1.5–3.2 °W (day 25–26). The lowest chlorophyll-a values of our study ( $0.10 \text{ mg m}^{-3}$ ) were found in this region at station 85 (day 26).

Further west, concentrations of chlorophyll-a sharply increased to  $3.3 \text{ mg m}^{-3}$  in an area from 52.0°S 8.8°W (day 27) to 50.9°S, 13.1°W (day 33). Blooms in this more land-remote region of the ACC have been previously documented, possibly fuelled by iron input from South Georgia to the east (Venables and Meredith, 2009). Sea surface temperature and salinity, in the mesoscale survey area, were relatively stable at about 2.5 °C and 33.88–33.90, respectively, until station 87 at about 50.8°S (day 33), where a distinct warming (3.5–4.0 °C) and freshening (33.80) was evident and was largely sustained for the remainder of the survey west of the Mid-Atlantic Ridge. High chlorophyll-a concentrations ( $\geq 1 \text{ mg m}^{-3}$ ) were measured throughout the mesoscale survey area.

Continuing westwards of the Mid-Atlantic Ridge towards the island of South Georgia (54–55°S, 36–37 °W), the greatest freshening (salinity of 32.18) was observed, relative to the whole survey region, due to locally warm, shallow shelf waters of South Georgia (day 54). Northwards, a strong gradient in sea surface temperature was present from about 3.3 °C to 4.3 °C, at 52.74 °S in the central Georgia Basin, to just over 7 °C by 50.81°S (day 55). From this point, a second mesoscale survey of 30 hydrographic station occupations was carried out at 48.5–51.5°S, 37–39.5°W (Fig. 1).

Large fluctuations in sea surface temperature and salinity were evident throughout the 6 day survey (Fig. 2a). Surface waters in the eastern part of the grid (stations 145, 146, 153) were typically warm (Fig. 4a) and slightly more saline (Fig. 4b); those in the west (stations 152, 158, 159, 164, 165, 170, 173) were cooler (Fig. 4a) and slightly fresher (Fig. 4b). Winter Water potential temperatures had properties of AAZ waters and revealed the presence of a cold-core cyclonic structure across most of the grid (Strass et al., in this issue). Warmer waters along the northern and eastern boundaries had temperature minima exceeding 2 °C, hence north of the PF, accompanied by a slight sub-surface salinity minimum showing that the SAF is in close proximity (Strass et al., in this issue). These features reflect the high levels of mesoscale activity in the region that have been previously well documented (Orsi et al., 1995; Meredith et al., 2003). Surface chlorophyll-a in the Georgia Basin grid was highly variable with patches of high and low concentrations in close proximity (Figs. 2 and 3). A surface water chlorophyll-a maximum for the entire survey of  $3.8 \text{ mg m}^{-3}$  was observed in the southern part of the grid at 50.8°S 38.2°W at station 156 (day 57) (Fig. 2b). Other notable chlorophyll-a peaks (chlorophyll-a  $\geq 2 \text{ mg m}^{-3}$ ) occurred at stations 144 (day 55), 159 (day 58) and 174 (day 61).

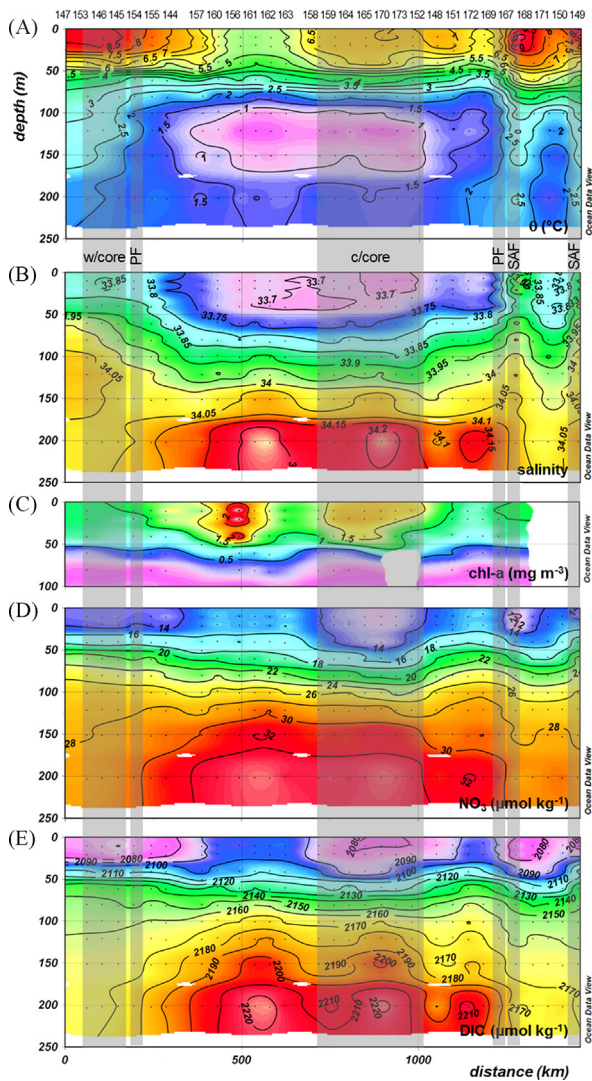


**Fig. 5.** Upper ocean distributions of potential temperature ( $\theta$ , °C), salinity, chl- $a$  ( $\text{mg m}^{-3}$ ),  $\text{NO}_3$  ( $\mu\text{mol kg}^{-1}$ ) and DIC ( $\mu\text{mol kg}^{-1}$ ) for the Georgia Basin. Station numbering at the top in the order shown in Fig. 4 and vertical grey columns indicate the location of the warm (w/core) and cold (c/core) cores.

### 3.2. Summertime $\text{CO}_2$ disequilibrium and seasonal DIC deficits

Surface waters were predominantly undersaturated across the region of investigation in the South Atlantic (Fig. 2c). Distinctly large  $\text{CO}_2$  disequilibrium was measured across the Subtropical Front (STF) (day 9–10). Oceanic  $\text{CO}_2$  saturation increased towards equilibrium levels with a steeper gradient at the SAF near station 65 (day 14–15). High oversaturation occurred near station 85 to create a regional maximum of  $f\text{CO}_2$  of  $3 \mu\text{atm}$  and efflux of  $\text{CO}_2$  (day 26). Surface waters throughout the mesoscale survey to the west Mid-Atlantic Ridge (stations 91–142) remained consistently undersaturated with relatively high  $\text{CO}_2$  disequilibrium around  $-40 \mu\text{atm}$ . Variable and strong  $\text{CO}_2$  disequilibrium was evident along the shelf and downstream of the island of South Georgia during the Georgia Basin mesoscale survey (stations 144–173). Greatest  $\text{CO}_2$  disequilibrium of  $-78 \mu\text{atm}$  in the local region occurred in the southwestern part of the grid (stations 156, 161, 162) (Fig. 4a). Upon completion of the mesoscale survey the ship steamed through surface waters of substantial  $\text{CO}_2$  disequilibrium in the south-western Georgia Basin, reaching a minimum for the study period of  $-120 \mu\text{atm}$  at  $52.30^\circ\text{S}$ ,  $40.89^\circ\text{W}$  (day 65). During the westward passage towards the Falkland Islands, oceanic  $\text{CO}_2$

disequilibrium returned to equilibrium levels with respect to atmospheric  $\text{CO}_2$ .

Wind speed ( $u_{10}$ ) from shipboard data and re-analysis data varied strongly along the cruise track (Fig. 2d). Instantaneous shipboard winds depicted fine scale fluctuations and had a mean value of  $10.6 \pm 3.8 \text{ m s}^{-1}$  ( $n=57,535$ ), ranging from  $1.2 \text{ m s}^{-1}$  during calm periods to over  $23.5 \text{ m s}^{-1}$  during storm events encountered between stations 67 and 69 (day 14), between stations 85 and 86 (day 28) and between stations 106 and 107 (day 38). Moderate to strong winds of  $10\text{--}17 \text{ m s}^{-1}$  prevailed along the cruise track. Wind speeds determined from the NCEP re-analysis product for January, February and March gave monthly mean values of  $10.8 \text{ m s}^{-1}$ ,  $10.0 \text{ m s}^{-1}$  and  $7.9 \text{ m s}^{-1}$ , respectively, i.e., generally lower than that measured onboard where the mean wind speed decreased each month.

The whole region was (on average) a moderate instantaneous sink of atmospheric  $\text{CO}_2$  of  $7.9 \text{ mmol m}^{-2} \text{ d}^{-1}$ . Oceanic  $\text{CO}_2$  uptake was generally lower across the SAZ and PFZ ( $0\text{--}14 \text{ mmol m}^{-2} \text{ d}^{-1}$ ) whereas strong  $\text{CO}_2$  sinks ( $\leq 57 \text{ mmol m}^{-2} \text{ d}^{-1}$ ) occurred south of the PFZ for all other regions (Fig. 2e). Moderate  $\text{CO}_2$  source waters of  $3\text{--}4 \text{ mmol m}^{-2} \text{ day}^{-1}$  were observed around station 85 (day 26–27) and over the Falkland Islands shelf at  $53.62^\circ\text{S}$   $55.16^\circ\text{W}$  (day 68). Intense oceanic  $\text{CO}_2$  sinks exceeding  $40 \text{ mmol m}^{-2} \text{ d}^{-1}$  were evident between stations 85 and 86 (day 28), between stations 106 and 107 (day 38) and at the south-western edge of the Georgia Basin,  $52.42^\circ\text{S}$ ,  $41.85^\circ\text{W}$ , (day 65), typically co-located with the storm events and largest  $\text{CO}_2$  disequilibrium. The corresponding value of the  $\text{CO}_2$  sink using NCEP wind speed averages was slightly less at  $6.7 \text{ mmol m}^{-2} \text{ d}^{-1}$ . Fluxes of  $\text{CO}_2$  determined from re-analysis data averaged per month give a more representative view of  $\text{CO}_2$  uptake as effects of short term storm events and calm periods are removed. Thus, the  $\text{CO}_2$  flux values more closely follow the variations in  $\text{CO}_2$  disequilibrium and that, with respect to monthly mean wind speeds, the data show that the region was a moderate sink of atmospheric  $\text{CO}_2$ .

The DIC deficit in the upper ocean reflects the spring–summer seasonal depletion of inorganic carbon up until the moment of sampling with respect to DIC concentrations at 100 m depth. The DIC deficit was generally small along the  $10^\circ\text{E}$  section (day 11–21), with the lowest values for the whole cruise (close to  $0 \text{ mol m}^{-2}$  at several stations, Fig. 2f). There was a gradual southward increase of DIC depletion with a regional maximum of  $2.0 \text{ mol m}^{-2}$  at station 83 (Table 1). In the mesoscale survey to the west of the Mid-Atlantic Ridge DIC deficits slightly increased and varied consistently between  $0.2 \text{ mol m}^{-2}$  and  $2.5 \text{ mol m}^{-2}$  throughout the whole survey (day 26–50). The DIC deficit further increased to  $2.9\text{--}5.1 \text{ mol m}^{-2}$  during the Georgia Basin mesoscale survey, downstream of South Georgia (day 55–61). The greatest DIC deficits occurred in the western part of the grid (stations 159, 165, 170, 173) reaching a maximum value of  $5.1 \text{ mol m}^{-2}$  at station 173 (Table 1). The higher DIC deficits coincided with the greatest degree of (more negative)  $\text{CO}_2$  disequilibrium (Fig. 2c and f). It is noted that DIC deficits could only be determined at the sites of hydrographic stations and that large  $\text{CO}_2$  disequilibrium occurred close to the beginning (day 10) and end of the survey (days 65–66), where no DIC data is available.

The nitrate deficit in the upper ocean reflects the seasonal biological depletion of nitrate. Nitrate deficits largely followed the DIC deficits, with lower values along the  $10^\circ\text{E}$  section and higher values in the Georgia Basin (Fig. 2f). The seasonal depletion of DIC as a result of net biological uptake is inferred from nitrate deficits using the Redfield ratio for C:N (106:16; Redfield et al., 1963), where the difference between measured and calculated DIC deficit can indicate the influence of gas exchange. However, the Redfield ratio has been shown to be variable and hence the calculated difference is strongly dependent on the C:N ratio used (Anderson

and Sarmiento, 1994). All warm core stations had a lower calculated (from nitrate deficits) versus measured DIC deficit, indicating an input of DIC through atmospheric CO<sub>2</sub> uptake. In contrast, most cold core stations had a higher calculated DIC deficit, resulting from a loss of DIC through CO<sub>2</sub> release from the ocean.

### 3.3. Identification and characterisation of mesoscale features

Satellite sea surface topography and chlorophyll-a (Fig. 3) revealed the location of the SAF passing to the north of the Georgia Basin and a large meander of the PF dominating the central part of the basin (Fig. 3). This was confirmed by shipboard potential temperature, salinity and potential density that showed a large cyclonic cold core eddy associated with the PF meander (Strass et al., in this issue). Cold, fresh surface waters and shoaling of the isotherms and isohalines in the upper 250 m (Figs. 5a and 5b) were associated with the PF, passing to the north of stations 144, 156, 161, 162. The Winter Water potential temperature minima were colder than 1.5 °C and located at around 200 m depth. The cold core eddy could be identified by cooler and slightly fresher surface waters with a cyclonic motion (Fig. 4a and b) and shoaling of the isotherms in the western part of the grid at stations 152, 159, 164, 165, 170, 173. Surface waters with high chlorophyll-a concentrations (1.5 mg m<sup>-3</sup>) become entrained into the large meander of the PF, with elevated concentrations observed to a depth of 50 m (Fig. 5c), and consistently trace the direction of the contours of dynamic height (Fig. 3). Productive (high chlorophyll-a) waters of the PF feed into the cold core eddy.

Warmer water to the north and east of the basin from the main flow and meanders in the SAF, respectively, emulated an anticyclonic warm core on the eastern margin of the mesoscale survey (Strass et al., in this issue). Maxima in sea surface temperature (11.7 °C) and salinity (34.11) occurred at station 167 (day 60) and secondary peaks (10.3 °C, 33.96) at station 149 (day 56) in the north of the grid (Fig. 4a). Considerable deepening of the isotherms and isohalines and intersection of 2 °C isotherm below 200 m confirmed that stations 149 and 167 are north of the PF, in the PFZ, and reflect characteristics of the SAF (Fig. 5a). Relative to surrounding waters of the AAZ, surface waters within the warm core eddy structure were typically warm and saline with an anticyclonic motion (Strass et al., in this issue), which encompassed stations 145, 146, 153 in the eastern part of the grid (Fig. 4a and b). The SAF was generally associated with lower chlorophyll-a concentrations, less than 0.5 mg m<sup>-3</sup> (Fig. 5c) that followed the meandering nature of the SAF to the north and PF to the south to form a smaller warm core structure in the east (Fig. 3). The cores of frontal water at 50–51°S in neighbouring patches (35–37°W, 37–39°W) thus simulated an eddy dipole in the Georgia Basin, where waters of the PFZ and AAZ are in close proximity with contrasting low and high chlorophyll-a concentrations, respectively.

## 4. Discussion

### 4.1. Mesoscale features and variability in oceanic CO<sub>2</sub> uptake

Satellite altimetry and ocean colour data showed the Georgia Basin to be a highly dynamic region (Fig. 3) with multiple mesoscale features due to the passage of the SAF in the north (~49°S) and the interaction of the PF (~51°S) with topography, most notably in the vicinity of South Georgia and Maurice Ewing Bank (Fig. 1). Shipboard measurements revealed this region to have fluctuations in sea surface temperature and salinity with high and variable surface chlorophyll-a concentrations accompanied by large (negative) CO<sub>2</sub> disequilibrium and substantial seasonal DIC depletion relative to the entire surveyed region (Fig. 2a, b, c and f).

The mesoscale survey in the Georgia Basin revealed the presence of a large meander in the PF entering the region in the south-western part of the survey grid, creating a cyclonic cold core. In the eastern part of the survey grid, a smaller anticyclonic warm core structure is evident from meanders in the main flow path of the SAF.

The cold core and warm core structure are not 'isolated' eddies but undergo some interaction with surrounding waters and modification to the water properties. However, as they reflect the characteristics of their respective end-member frontal waters, with distinct surface (temperature, salinity and chlorophyll-a) and upper ocean expressions (potential temperature and salinity), they are taken here to represent an eddy dipole. Stations 149, 167 are situated close to the SAF in the north and with water mass characteristics of the PFZ; stations 144, 156, 161, 162 are set within the large meander of the PF with water mass characteristics of the AAZ; these two sets of stations are taken as end-member stations in interpreting the effects of eddy structures on the CO<sub>2</sub> uptake and the distribution of DIC in the upper ocean.

The summertime CO<sub>2</sub> disequilibrium across the Georgia Basin reflects the influence of the mesoscale activity with consistently high but variable CO<sub>2</sub> disequilibrium (Fig. 4c). Relative to the PFZ end-member stations (149, 167), the pre-conditioned (warm, salty, low chlorophyll-a) waters of the SAF meander that feed the warm core structure were modified through sea surface cooling (Fig. 4a) and freshening (Fig. 4b). Such changes led to enhanced CO<sub>2</sub> disequilibrium and uptake of atmospheric CO<sub>2</sub>. The strongest CO<sub>2</sub> disequilibrium (–86 μatm) occurred near the main path of the PF at station 156, which coincided with the highest chlorophyll-a values (3.8 mg m<sup>-3</sup>).

The relatively low nitrate concentrations of waters of the PFZ are drawn down into the water column by deepening of the nutricline concurrent with the thermocline (Fig. 5d). Despite low/moderate chlorophyll-a concentrations in the upper 50 m, nitrate and DIC were relatively depleted within the warmest waters near the surface. Low concentrations of nitrate and DIC characterised the warm core structure throughout the upper 250 m, as summertime productive waters of the euphotic zone that were depleted in nitrate and DIC were drawn down in-line with deepening isotherms, i.e., the depth of the 2170 μmol kg<sup>-1</sup> contour was deepened by about 100–150 m (Fig. 5e).

Relative to the AAZ end-member stations (144, 156, 161, 162), the northward transport of pre-conditioned (cold, fresh, high chlorophyll-a) water into the cold core experienced warming (Fig. 4a) and thermodynamic CO<sub>2</sub> saturation (Fig. 4c). Warming of surface waters acts to compensate the strong biological CO<sub>2</sub> uptake in the productive cold core, which can be seen in the reduction of the CO<sub>2</sub> disequilibrium originally associated with the AAZ source waters (Fig. 4c). The distinct cold and salty waters below 100 m of the AAZ are transferred to and thus used to identify the cold core eddy-like feature displaying distinct perturbations to the upper 250 m of the water column across a diameter of ~400 km. Warming penetrated the upper 50 m with a slight deepening and strengthening of the thermocline (Fig. 5a). Distinct sub-surface potential temperature minima less than 1 °C were detected between 100–200 m across the cold core, retaining the distinct feature of the broad potential temperature minimum. Below the Winter Water potential temperature minimum, salty, nitrate- and DIC-rich water was upwelling along the shoaling isopycnals. Thus, high nitrate and DIC concentrations are projected/ transported towards the surface with maximal vertical gradients across the thermocline. However, surface nitrate and DIC values are rapidly reduced in the upper 50 m, co-incident with some of the highest chlorophyll-a values (second to those measured near the main flow of the PF to the south) where

chlorophyll-*a* concentrations exceeded  $1.5 \text{ mg m}^{-3}$  from the surface to 50 m depth (Fig. 5c).

Highest vertical gradients in DIC occurred across the thermocline from the base of the mixed layer to 120 m depth (Fig. 5e). The low concentrations of DIC within the shallow mixed layer (20 m) of the warm core increased by  $100 \mu\text{mol kg}^{-1}$  to around  $2170 \mu\text{mol kg}^{-1}$  at about 100 m, with little increase by 250 m depth. In contrast, the deeper mixed layers (20–50 m) of the cold core had slightly higher surface DIC concentrations that increased steadily from the base of the mixed layer to 120 m and then continued to increase towards  $2225 \mu\text{mol kg}^{-1}$  at 250 m depth. This pattern was concurrent in the nitrate distributions (Fig. 5d).

#### 4.2. Hotspots of carbon uptake in the ACC

Two principal carbon parameters are selected as criteria to assess whether an area represents a 'hotspot' of carbon uptake in terms of: (1) DIC deficits—the balance of uptake and input of inorganic carbon in the upper 100 m of the water column; (2)  $\text{CO}_2$  disequilibrium ( $\Delta f\text{CO}_2$ )—the summertime degree of (under-)saturation of the surface ocean with respect to atmospheric  $\text{CO}_2$ .

All  $\text{CO}_2$  disequilibrium along the cruise track ( $n=57,535$ ) and DIC deficits for each station ( $n=105$ ) were averaged to assess carbon cycling across the whole cruise track in the South Atlantic (Table 1). The whole trans-Atlantic survey region had (on average) moderate upper-ocean seasonal depletion in DIC of  $2.1 \pm 1.5 \text{ mol m}^{-2}$  and quite strong  $\text{CO}_2$  disequilibrium of  $-38 \pm 20 \mu\text{atm}$ . Hotspots are defined here by accounting for one standard deviation of each

parameter (DIC deficits and  $\Delta f\text{CO}_2$ ) as this reflects a quantitative assessment of the variability by considering the deviation from the mean of all summertime data in the whole surveyed region. Therefore, hotspots of carbon uptake have DIC deficits and  $\text{CO}_2$  disequilibrium exceeding  $3.6 \text{ mol m}^{-2}$  and  $-58 \mu\text{atm}$ , respectively (Table 1). Such hotspots were identified in 11 locations: stations 144, 145, 152, 156, 159, 161, 162, 164, 165, 170, 173; persistently in the cold core in the Georgia Basin (Fig. 6a). Air–sea  $\text{CO}_2$  fluxes are used to investigate further the transient summertime exchange of  $\text{CO}_2$  with the atmosphere due to the influence of *in-situ* wind speeds at the time of sampling and hence represent a snap-shot of  $\text{CO}_2$  uptake. The higher DIC deficits and strong  $\text{CO}_2$  disequilibrium in the warm and cold cores were frequently accompanied by moderate to high  $\text{CO}_2$  sinks (Fig. 6b and c), but the relationship between  $\text{CO}_2$  disequilibrium and the actual  $\text{CO}_2$  sink is weaker due to the additional wind speed variable. The  $\text{CO}_2$  flux determined from monthly averaged re-analysis wind speeds more closely followed the variations in  $\text{CO}_2$  disequilibrium due to the smoothing of short term wind speed fluctuations (storm and calm periods). This is a more representative view of the magnitude of summertime  $\text{CO}_2$  uptake in this region, highlighting the same patterns of enhanced  $\text{CO}_2$  uptake across the ACC and especially in the Georgia Basin.

DIC deficits rely on the assumption of no advection and mixing, which is not the case in the dynamic ACC (Naveira Garabato et al., 2004). Therefore, DIC deficits on a large spatial (basin wide) scale are better examined by taking into account the temporal differences, i.e., the time of sampling (Table 1). Satellite chlorophyll-*a* images of the months leading up to the survey (not shown) indicate elevated

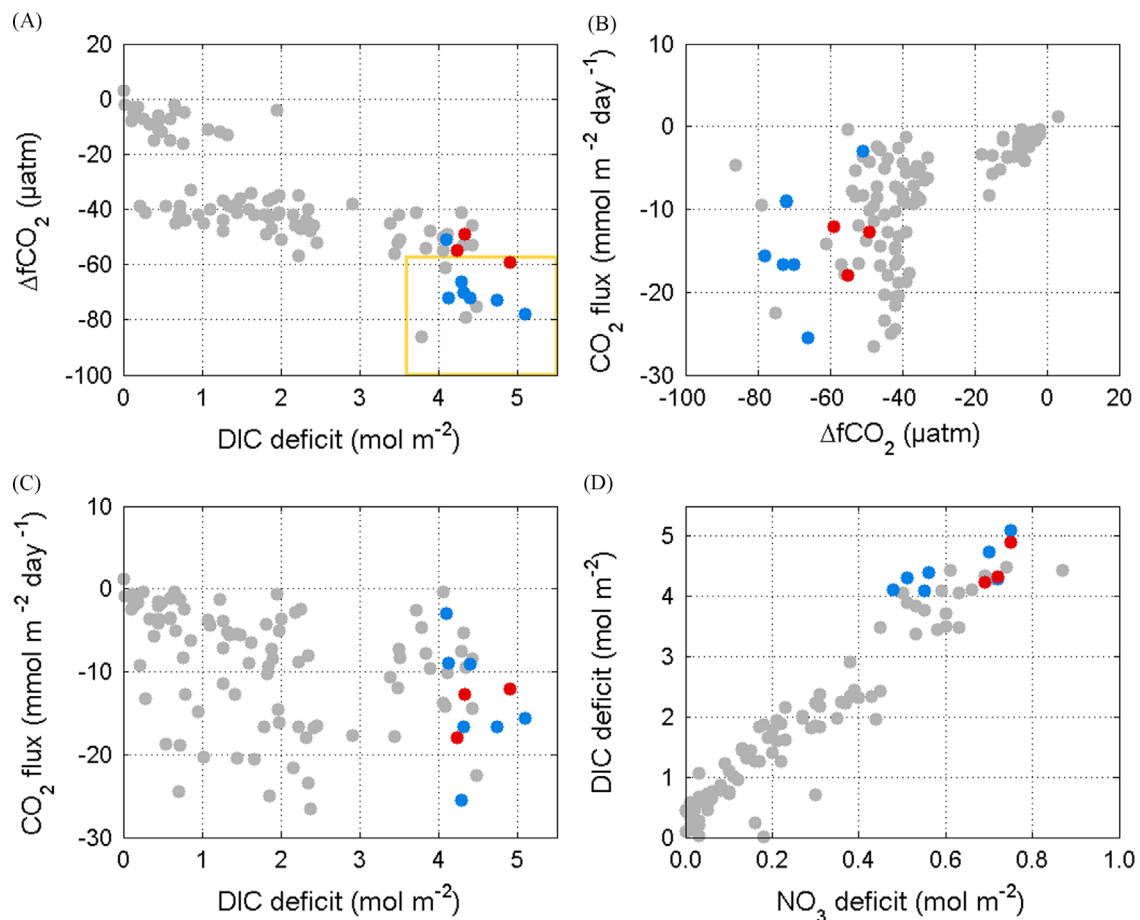


**Fig. 6.** Relationships for all data (grey), warm core (red) and cold core (blue) in the Georgia Basin for (a)  $\Delta f\text{CO}_2$  ( $\mu\text{atm}$ ) and DIC deficit ( $\text{mol m}^{-2}$ ), (b) air–sea  $\text{CO}_2$  flux ( $\text{mmol m}^{-2} \text{ d}^{-1}$ ) and DIC deficit ( $\text{mol m}^{-2}$ ), (c) air–sea  $\text{CO}_2$  flux ( $\text{mmol m}^{-2} \text{ d}^{-1}$ ) and  $\Delta f\text{CO}_2$  ( $\mu\text{atm}$ ), (d) DIC deficit ( $\text{mol m}^{-2}$ ) and  $\text{NO}_3$  deficit ( $\text{mol m}^{-2}$ ). The yellow box highlights 'hotspots' with respect to DIC deficit and  $\Delta f\text{CO}_2$ . (For interpretation of the references to colour in this figure legend, the reader is referred to the web version of this article.)

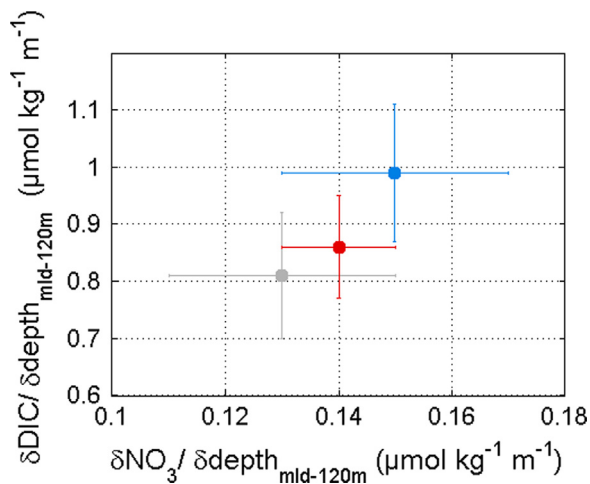


**Fig. 7.** DIC gradient ( $\delta\text{DIC}/\delta\text{depth}$ ,  $\mu\text{mol kg}^{-1} \text{d}^{-1}$ ) vs. nitrate gradient ( $\delta\text{NO}_3/\delta\text{depth}$ ,  $\mu\text{mol kg}^{-1} \text{d}^{-1}$ ) between the base of the summer mixed layer (MLD, m) and 100 m for all stations in the Georgia Basin mesoscale survey.

chlorophyll-*a*, with increased light levels, occurring from early spring, i.e., October 2011, thus 1 October 2011 is taken as the start of the growing season. DIC deficits determined by *in-situ* sampling are normalised to rate of change of DIC per day after the start of the growing (productive) season ( $t_0=1$  October 2011). The rate of consumption of DIC over the length of the growing season reached maxima of  $33.5 \text{ mmol m}^{-2} \text{ day}^{-1}$  and  $33.1 \text{ mmol m}^{-2} \text{ day}^{-1}$  in the warm and cold eddy cores, respectively, relative to the rate of depletion of  $19.3\text{--}29.7 \text{ mmol DIC m}^{-2} \text{ day}^{-1}$  in the surrounding waters of the Georgia Basin. This confirms that the cold core and warm core are areas of enhanced biologically-driven DIC uptake.

As both the warm and cold cores had steadily increasing DIC concentrations between the base of the mixed layer and 120 m, this can be used to investigate the vertical gradients in both DIC and nitrate. Changes in nitrate along the gradient can be used as an indicator of biological DIC uptake (Fig. 6d). The rate of change of DIC ( $1 \mu\text{mol kg}^{-1} \text{m}^{-1}$ ) relative to nitrate ( $0.15 \mu\text{mol kg}^{-1}$ ) shows that high concentrations of DIC introduced at the base of the thermocline are rapidly reduced in the depth range between the base of summer mixed layer and 120 m, indicating the strong effect of biological carbon uptake within the cold core eddy that counteracts the input of DIC-rich waters from below (Fig. 7). Comparing DIC deficits determined from DIC measurements to those calculated from nitrate deficits could suggest an additional loss of DIC within the cold core through  $\text{CO}_2$  release to the atmosphere, however this result is dependent on the C:N ratio used.

The cold core and warm core eddy structures in the Georgia Basin represent hotspots of carbon uptake during the summer, relative to the surrounding surveyed waters of the ACC. A suggested mechanism is based on the Ekman eddy pumping theory, as postulated by McGillicuddy et al. (1998), and is shown schematically in Fig. 8. Waters of the cyclonic cold core eddy can become seeded with productive (high chlorophyll-*a*) waters from the AAZ where an enhanced biological response occurs through upwelled (micro-)nutrients into the euphotic zone. Upwelled deep waters would also supply the upper ocean with DIC. However, it is postulated that DIC delivered along the thermocline of the cold core eddy are largely compensated by the concurring high rates of biological carbon depletion that occur in the euphotic zone.

The horizontal entrainment of low DIC surface waters (from spring–summer biological carbon uptake in the euphotic zone) of the PFZ downwell within the anticyclonic warm core to yield relative DIC-depletion in the upper water column (Fig. 8). The impact of cold cores shed from meanders of the PF could further

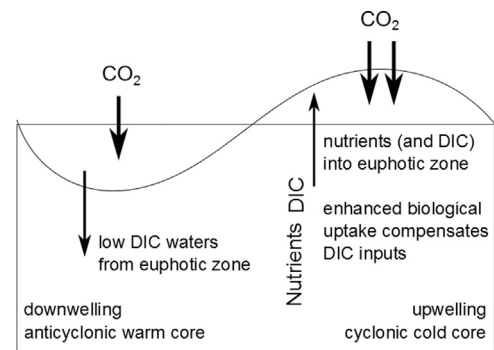


**Fig. 8.** Summary of proposed eddy (Ekman) pumping mechanism, highlighting the main flows of  $\text{CO}_2$  and DIC, in the cyclonic cold core and anticyclonic warm core eddy structures in the Georgia Basin.

enhance the carbon uptake capacity of this region as highly productive waters of the AAZ seed the upper ocean and upwelled (micro-)nutrients resupply the euphotic zone with nutrients. When the uptake ratio C:Fe in the surface is higher than the C:Fe ratio of upwelled deeper waters, this mechanism can enhance seasonal carbon deficits by stimulating a biological response and negating the effect of input of carbon-rich deep waters. Accompanied by strong  $\text{CO}_2$  disequilibrium, significant instantaneous oceanic  $\text{CO}_2$  sinks can ensue in the presence of high winds (up to  $-25.5 \text{ mmol m}^{-2} \text{ d}^{-1}$ ), which are shown to be only slightly dampened at this location, i.e.  $-13.6 \text{ mmol m}^{-2} \text{ d}^{-1}$ , when removing fluctuations by using wind speed monthly means to compute the  $\text{CO}_2$  fluxes. The results described here indicate that the northward deflection of persistent meanders of the PF and eddy shedding could displace a DIC-deficient mixed layer towards the PFZ, the site of Antarctic Intermediate Water formation, subsequently enhancing the subduction of low carbon waters into the ocean interior.

Waters downstream of South Georgia, in the southern Georgia Basin, have previously been identified as sites of high biological carbon uptake (Jones et al., 2012; *in press*) within the extensive phytoplankton blooms that develop annually (Korb et al., 2004; Borrione and Schlitzer, 2013). In a wider Southern Ocean context, the DIC deficits in the upper 100 m of the eddy structures in the Georgia Basin ( $4.1\text{--}5.1 \text{ mol m}^{-2}$ ) are some of the largest in ice-free waters of the Southern Ocean; compared to  $2.2 \text{ mol m}^{-2}$  in the central Scotia Sea ( $56\text{--}58^\circ\text{S}$ ,  $37\text{--}43^\circ\text{W}$ ) (Jones et al., 2012),  $3.4 \text{ mol m}^{-2}$  by the Crozet plateau, Indian Ocean ( $45\text{--}47^\circ\text{S}$ ,  $49\text{--}53^\circ\text{E}$ ) (Bakker et al., 2007),  $4.6 \text{ mol m}^{-2}$  in the central Georgia Basin ( $5\text{--}54^\circ\text{S}$ ,  $38\text{--}42^\circ\text{E}$ ) (Jones et al., 2012) and  $1.2\text{--}10.8 \text{ mol m}^{-2}$  in the Ross Sea ( $77^\circ\text{S}$ ,  $169\text{--}187^\circ\text{E}$ ) (Bates et al., 1998; Sweeney et al., 2000).

## 5. Conclusion

Cold core and warm core eddy structures created hotspots of carbon uptake in the ACC during austral summer. The most intense undersaturation in oceanic  $\text{CO}_2$  of  $-78 \mu\text{atm}$  and substantial seasonal deficits in DIC of  $5.1 \text{ mol m}^{-2}$  occurred within a large cyclonic cold core in the Georgia Basin, downstream of the island of South Georgia. Eddy (Ekman) pumping is proposed as a mechanism where productive (high chlorophyll-*a*) waters from a meander in the Polar Front seed the cold core, which is subsequently resupplied with upwelled (micro-)nutrients and sustained biological carbon uptake follows. Nitrate deficits along the thermocline indicate rapid biological assimilation of DIC that counteracts inputs from carbon-rich deep waters. High wind speeds created a strong instantaneous sink for atmospheric  $\text{CO}_2$  of

–25.5 mmol m<sup>-2</sup> day<sup>-1</sup> in the cold core eddy. The anticyclonic warm core structure also showed enhanced carbon uptake through the horizontal entrainment of low DIC surface waters (spring–summer biological carbon uptake) from the Polar Frontal Zone, which downwell within the warm core to cause relative DIC-depletion in the upper water column.

The formation and northward projection of cold core eddies from the PF can displace DIC-deficient mixed layer towards the site of Antarctic Intermediate Water formation in the Polar Frontal Zone. Subduction of intermediate waters enables low carbon waters to permeate the ocean interior. Therefore, eddy pumping mechanisms in the ACC could enhance CO<sub>2</sub> drawdown into the deep ocean. This study does not attempt to attribute the observations definitively to eddy mechanisms but provides an insight on how mesoscale activity, that includes eddies, influences the summertime and seasonal uptake of CO<sub>2</sub>. From this observational perspective, a base can be drawn in order to better assess the role of eddies in carbon cycling in the ACC.

## Acknowledgements

The authors would like to thank the Captain, officers, crew and scientists onboard FS *Polarstern* during Antarctic expedition ANT-XXVIII/3. Extended thanks to Christoph Völker (AWI) for assistance with NCEP re-analysis wind data and Hugh Venables (BAS) for numerous helpful discussions. MODIS-Aqua chlorophyll-a data were obtained from the SeaWiFS Project, NASA Goddard Space Flight Centre. This work partly supported by the Deutsche Forschungsgemeinschaft (DFG) in the framework of the priority programme “Antarctic Research with comparative investigations in Arctic ice areas” by a grant to M. Hoppema (HO 4680/1). Partial support to M. Hoppema and H.J.W. de Baar was received from EU FP7 project CARBOCHANGE (European Community’s 7th Framework Program, Grant agreement no. 264879). The authors acknowledge the constructive comments by the editors and an anonymous reviewer that greatly helped to improve the manuscript.

## References

Allen, C.B., Kanda, J., Laws, E.A., 1996. New production and photosynthetic rates within and outside a cyclonic mesoscale eddy in the North Pacific subtropical gyre. *Deep-Sea Res.* 1 43, 917–936.

Anderson, L.A., Sarmiento, J.L., 1994. Redfield ratios of remineralization determined by nutrient data analysis. *Glob. Biogeochem. Cycles* 8, 65–80. <http://dx.doi.org/10.1029/93GB03318>.

Atkinson, A., Whitehouse, M.J., Priddle, J., Cripps, G.C., Ward, P., Brandon, M.A., 2000. South Georgia, Antarctica: a productive, cold water, pelagic ecosystem. *Mar. Ecol. Prog. Ser.* 216, 279–308.

Bakker, D.C.E., Nielsdóttir, M.C., Morris, P.J., Venables, H.J., Watson, A.J., 2007. The island mass effect and biological carbon uptake for the subantarctic Crozet Archipelago. *Deep-Sea Res.* II 54, 2174–2190.

Bates, N.R., Hansell, D.A., Carlson, C.A., 1998. Distributions of CO<sub>2</sub> species, estimates of net community production, and air–sea CO<sub>2</sub> exchanges in the Ross Sea polynya. *J. Geophys. Res.* 103, 2883–2896.

Böning, C.W., Dispert, A., Visbeck, M., Rintoul, S.R., Schwarzkopf, U., 2008. The response of the Antarctic Circumpolar Current to recent climate change. *Nat. Geosci.* 1, 864–869.

Borrione, I., Schlitzer, R., 2013. Distribution and recurrence of phytoplankton blooms around South Georgia, Southern Ocean. *Biogeosciences* 10, 217–231.

Dickson, A.G., 1981. An exact definition of total alkalinity and a procedure for the estimation of alkalinity and total inorganic carbon from titration data. *Deep-Sea Res.* 28, 609–623.

Dickson, A.G. In: Guide to best practices for ocean CO<sub>2</sub> measurements (eds. A.G. Dickson, C.L. Sabine and J.R. Christian). PICES Special Publication 3, pp. 1–191.

Dufois, F., Hardman-Mountford, N.J., Greenwood, J., Richardson, A.J., Feng, M., Herbette, S., Matear, R., 2014. Impact of eddies on surface chlorophyll in the Southern Indian Ocean. *J. geophys. Res.* 119, 8061–8077. <http://dx.doi.org/10.1002/2014JC010164>.

Falkowski, P., Ziemann, D., Kolber, Z., Bienfang, P., 1991. Role of eddy pumping in enhancing primary production in the ocean. *Nature* 353, 55–58.

Hartman, B., Hammond, D.E., 1985. Gas exchange in San Francisco Bay. *Hydrobiologia* 129, 59–68.

Hauck, J., Völker, C., Wang, T., Hoppema, H., Losch, M., Wolf-Gladrow, D.A., 2013. Seasonally different carbon flux changes in the Southern Ocean in response to the Southern Annular Mode. *Glob. Biogeochem. Cycles* 27, 1236–1245. <http://dx.doi.org/10.1002/2013GB004600>.

Hoppe, C.J.M., Klaas, C., Ossebaar, S., Soppa, M.A., Cheah, W., Rost, B., Wolf-Gladrow, D., Bracher, A., Hoppema, M., Strass, V. and Trimborn, S., Controls of primary production in two phytoplankton blooms in the Antarctic Circumpolar Current. This issue.

Johnson, K.M., Sieburth, J.M., Williams, P.J.L., Brandstrom, L., 1987. Coulometric total carbon dioxide analysis for marine studies—automation and calibration. *Mar. Chem.* 21, 117–133.

Jones, E.M., Bakker, D.C.E., Venables, H.J., Hardman-Mountford, N.J., 2015. Seasonal cycle of CO<sub>2</sub> from the sea ice edge to island blooms in the Scotia Sea, Southern Ocean. *Mar. Chem.* . <http://dx.doi.org/10.1016/j.marchem.2015.06.031>, in press

Jones, E.M., Bakker, D.C.E., Venables, H.J., Watson, A.J., 2012. Dynamic seasonal cycling of inorganic carbon downstream of South Georgia, Southern Ocean. *Deep-Sea Res.* II 59–60, 2–35.

Kalnay, E., Kanamitsu, M., Kistler, R., Collins, W., Deaven, D., Gandin, L., Iredell, M., Saha, S., White, G., Woollen, J., Zhu, Y., Leetmaa, A., Reynolds, R., Chelliah, M., Ebisuzaki, W., Higgins, W., Janowiak, J., Mo, K.C., Ropelewski, C., Wang, J., Jenne, R., Joseph, D., 1996. The NCEP/NCAR 40-year reanalysis project. *Bull. Amer. Meteor. Soc.* 77, 437–470, doi: [http://dx.doi.org/10.1175/1520-0477\(1996\)077<0437:TNYRP>2.0.CO;2](http://dx.doi.org/10.1175/1520-0477(1996)077<0437:TNYRP>2.0.CO;2).

Kimura, S., Kasai, A., Nakata, H., Sugimoto, T., Simpson, J.H., Cheok, J.V.S., 1997. Biological productivity of meso-scale eddies caused by frontal disturbances in the Kuroshio. *ICES J. Mar. Sci.* 54, 179–192.

Klein, P., Lapeyre, G., 2009. The oceanic vertical pump induced by mesoscale and submesoscale turbulence. *Annu. Rev. Mar. Sci.* 1, 351–375.

Knap, A., A. Michaels, A. Close, H. Ducklow and A. Dickson (eds.), 1996. Protocols for the Joint Global Ocean Flux Study (JGOFS) Core Measurements. JGOFS Report Nr. 19, vi+170 pp. Reprint of the IOC Manuals and Guides No. 29, UNESCO 1994.

Korb, R.E., Whitehouse, M.J., 2004. Contrasting primary production regimes around South Georgia, Southern Ocean: large blooms versus high nutrient, low chlorophyll waters. *Deep-Sea Res.* I 51, 721–738.

Korb, R.E., Whitehouse, M.J., Ward, P., 2004. SeaWiFS in the southern ocean: spatial and temporal variability in phytoplankton biomass around South Georgia. *Deep-Sea Res.* II 51, 99–116.

Law, R.M., Matear, R.J., Francey, R.J., 2008. Comment on “Saturation of the Southern Ocean CO<sub>2</sub> sink due to recent climate change”. *Science* 319, 570. <http://dx.doi.org/10.1126/science.1149077>.

Le Quééré, C., Rödenbeck, C., Buitenhuis, E.T., Conway, T.J., Langenfelds, R., Gomez, A., Labuschagne, C., Ramonet, M., Nakazawa, T., Metz, N., Gillett, N., Heimann, M., 2007. Saturation of the Southern Ocean CO<sub>2</sub> sink due to recent climate change. *Science* 316, 1735.

Lee, M.-M., Williams, R.G., 2000. The role of eddies in the isopycnic transfer of nutrients and their impact on biological production. *Journal of Marine Res.* 58, 895–917.

Lévy, M., 2003. Mesoscale variability of phytoplankton and of new production: impact of the large scale nutrient distribution. *J. Geophys. Res.* 108, 3358.

Lovenduski, N.S., Gruber, N., Doney, S.C., 2008. Toward a mechanistic understanding of the decadal trends in the Southern Ocean carbon sink. *Glob. Biogeochem. Cycles* 22, GB3016. <http://dx.doi.org/10.1029/2007gb003139>.

Marshall, J., Speer, K., 2012. Closure of the meridional overturning circulation through Southern Ocean upwelling. *Nat. Geosci.* 5, 171–180.

McGillicuddy Jr, D.J., Robinson, A.R., Siegel, D.A., Jannasch, H.W., Johnson, R., Dickey, T.D., McNeil, J., Michaels, A.F., Knap, A.H., 1998. Influence of mesoscale eddies on new production in the Sargasso Sea. *Nature* 394, 263–266.

McGillicuddy, D.J., Robinson, A.R., 1997. Eddy-induced nutrient supply and new production in the Sargasso Sea. *Deep-Sea Res.* I 44, 1427–1450.

Meredith, M.P., Watkins, J.L., Murphy, E.J., Cunningham, N.J., Wood, A.G., Korb, R., Whitehouse, M.J., Thorpe, S.E., Vivier, F., 2003. An anticyclonic circulation above the Northwest Georgia Rise, Southern Ocean. *Geophys. Res. Lett.* 30, 2061. <http://dx.doi.org/10.1029/2003GL018039>.

Moore, J.K., Abbott, M.R., 2000. Phytoplankton chlorophyll distributions and primary production in the Southern Ocean. *J. Geophys. Res.* 105, 28709–28722.

Naveira Garabato, A.C., Polzin, K.L., King, B.A., Heywood, K.J., Visbeck, M., 2004. Widespread intense turbulent mixing in the Southern Ocean. *Science* 303, 210–213.

Nightingale, P.D., Malin, G., Law, C.S., Watson, A.J., Liss, P.S., Liddicoat, M.I., Boutin, J., Upstill-Goddard, R.C., 2000. In situ evaluation of air–sea gas exchange parameterizations using novel conservative and volatile tracers. *Glob. Biogeochem. Cycles* 14, 373–387.

Orsi, A.H., Whitworth, T., Nowlin, W.D., 1995. On the meridional extent and fronts of the Antarctic Circumpolar Current. *Deep-Sea Res.* I 42, 641–673.

Pollard, R.T., Lucas, M.L., Read, J.F., 2002. Physical controls on biogeochemical zonation in the Southern Ocean. *Deep-Sea Res.* II 49, 3289–3305.

Redfield, A.C., Ketchum, B.H., Richards, F.A., 1963. The influence of organisms on the composition of seawater. In: Hill, M.N. (Ed.), *The Sea*, Vol. 2. Wiley, New York, pp. 26–77, *The Composition of Seawater*.

Rintoul, S., Hughes, C. and Olbers, D. 2001. “The Antarctic circumpolar current system.” In: *Ocean Circulation and Climate/G. Siedler, J. Church and J. Gould, eds. New York: Academic Press.* pp. 271–302.

Robinson, A.R., McGillicuddy, D.J., Calman, J., Ducklow, H.W., Fasham, M.J.R., Hoge, F. E., Leslie, W.G., McCarthy, J.J., Podewski, S., Porter, D.L., Saure, G., Yoder, J.A.,

1993. Mesoscale and upper ocean variabilities during the 1989 JGOFS bloom study. *Deep-Sea Res. II* 40, 9–35.
- Saraceno, M., Provost, C., 2012. On eddy polarity distribution in the southwestern Atlantic. *Deep-Sea Res. I* 69, 62–69.
- Siegel, D.A., McGillicuddy Jr., D.J., Fields, E.A., 1999. Mesoscale eddies, satellite altimetry, and new production in the Sargasso Sea. *J. Geophys. Res.* 104 (C6). <http://dx.doi.org/10.1029/1999JC900051> 359–13,379.
- Smith, I.J., Stevens, D.P., Heywood, K.J., Meredith, M.P., 2010. The flow of the Antarctic Circumpolar Current over the North Scotia Ridge. *Deep-Sea Res. I* 57, 14–28.
- Sokolov, S., Rintoul, S.R., 2007. On the relationship between fronts of the Antarctic Circumpolar Current and surface chlorophyll concentrations in the Southern Ocean. *J. Geophys. Res.* 112 (C07030). <http://dx.doi.org/10.1029/2006JC004072>.
- Strass, V.H., Naveira Garabato, A.C., Pollard, R.T., Fischer, H.J., Hense, I., Allen, J.T., Read, J.F., Leach, H., Smetacek, V., 2002. Mesoscale frontal dynamics: shaping the environment of primary production in the Antarctic Circumpolar Current. *Deep-Sea Res. II* 49, 3735–3769.
- Strass, V.H., 1992. Chlorophyll patchiness caused by mesoscale upwelling at fronts. *Deep-Sea Res.* 39, 75–96.
- Strass, V., Leach, H., Prandke, H., Donnelly, M., Bracher, A. and Wolf-Gladrow, D. The physical environmental conditions of biogeochemical differences along the ACC in the Atlantic Sector during late austral summer. This issue.
- Sweeney, C., Smith, W.O., Hales, B., Bidigare, R.R., Carlson, C.A., Codispoti, L.A., Gordon, L.I., Hansell, D., Millero, F.J., Park, M.-O.K., Takahashi, T., 2000. Nutrient and carbon removal ratios and fluxes in the Ross Sea, Antarctica. *Deep-Sea Res. II* 47, 3395–3421.
- Takahashi, T., Sutherland, S.C., Wanninkhof, R., Sweeney, C., Feely, R.A., Chipman, D. W., Hales, B., Friederich, G., Chavez, F., Sabine, C.L., Watson, A.J., Bakker, D.C.E., Schuster, U., Metzl, Yoshikawa-Inoue, H., Ishii, M., Midorikawa, T., Nojiri, Y., Körtzinger, Steinhoff, T., Hoppema, M., Olafsson, J., Arnarson, T.S., Tilbrook, B., Johannessen, T., Olsen, A., Bellerby, R., Wong, C.S., Delille, B., Bates, N.R., de Baar, H.J.W., 2009. Climatological mean and decadal change in surface ocean pCO<sub>2</sub>, and net sea-air CO<sub>2</sub> flux over the global oceans. *Deep-Sea Res. II* 56, 554–577.
- Takahashi, T., Olafsson, J., Goddard, J.G., Chipman, D.W., Sutherland, S.C., 1993. Seasonal variation of CO<sub>2</sub> and nutrients in the high latitude surface oceans—a comparative-Study. *Glob. Biogeochem. Cycles* 7, 843–878.
- Thompson, A.F., Heywood, K.J., Schmidtke, S., Stewart, A.L., 2014. Eddy transport as a key component of the Antarctic overturning circulation. *Nat. Geosci.* 7, 879–884.
- Trathan, P.N., Brandon, M.A., Murphy, E.J., Thorpe, S.E., 1997. Characterisation of the Antarctic Polar Frontal Zone to the north of South Georgia in summer 1984. *J. Geophys. Res.* 102, 10483–10497.
- Venables, H.J., Meredith, M.P., 2009. Theory and observations of Ekman flux in the chlorophyll distribution downstream of South Georgia. *Geophys. Res. Lett.* 36, L23610. <http://dx.doi.org/10.1029/2009GL041371>.
- Venables, H.J., Meredith, M.P., Atkinson, A., Ward, P., 2012. Fronts and habitat zones in the Scotia Sea. *Deep-Sea Res. II* 59–60, 14–24.
- Watson, A.J., Orr, J.C., 2003. Carbon dioxide fluxes in the global ocean. In: Fasham, M.J.R. (Ed.), *Ocean Biogeochemistry: The role of the Ocean Carbon Cycle in Global Change*. Springer-Verlag, Berlin.
- Weiss, R.F., Price, B.A., 1980. Nitrous-oxide solubility in water and seawater. *Mar. Chem.* 8, 347–359.
- Wolf-Gladrow, D. [Ed.], 2013. The Expedition of the Research Vessel "Polarstern" to the Antarctic in 2012 (ANT-XXVIII/3), Reports on Polar and Marine Research, 661, 190pp, Alfred-Wegener-Institut, Bremerhaven. <http://hdl.handle.net/10013/epic.41332>.
- Zickfeld, K., Fyfe, J.C., Eby, M., Weaver, A.J., 2008. Comment on "Saturation of the Southern Ocean CO<sub>2</sub> Sink Due to Recent Climate Change". *Science* 319, 570. <http://dx.doi.org/10.1126/science.1146886>.